sustainability

MDPI

Article

Dynamic Characteristics of Rock Holes with Gravel Sediment Drilled by Bit Anchor Cable Drilling

Kuidong Gao, Jihai Liu, Hong Chen, Xu Li * and Shuan Huang

College of Mechanical and Electronic Engineering, Shandong University of Science and Technology, Qingdao 266590, China; gaokuidong22@163.com (K.G.); ljhsdust@163.com (J.L.)
* Correspondence: lixu2017@sdust.edu.cn

Abstract: Gravel and sediment frequently build up in holes during the anchor cable installation process, which makes it harder to install the anchor cable and causes reinforcement to fail, which can lead to accidents. In this paper, a bit anchor setup approach is proposed to set up a drill bit at the front of the anchor cable to aid the anchor cable drilling. The feasibility of this approach is established with the aid of DEM-MBD joint simulation and proves the correctness of the simulation model. The major elements affecting drilling effectivity have been studied by the use of 'check + simulation'. The effects exhibit that the axial velocity and working aperture are negatively correlated with the drilling resistance of the anchor cable; the feed price is positively related to the anchor cable drilling resistance; with the increase in anchor cable pitch, the drilling resistance of the anchor cable changes into a hump shape. When the bit is 0.2 m from the backside of the hole, the particle pace vector at the decrease stop of the bit gives a conical distribution. This paper is of fantastic magnitude in relation to the environment-friendly setup of anchor cables and protection against disasters.

Keywords: anchor cable installation; disaster prevention; DEM-MBD joint simulation; bit anchor cable; dynamic characteristics

Citation: Gao, K.; Liu, J.; Chen, H.; Li, X.; Huang, S. Dynamic Characteristics of Rock Holes with Gravel Sediment Drilled by Bit Anchor Cable Drilling. *Sustainability* **2023**, *15*, 5956. https://doi.org/10.3390/su15075956

Academic Editors: Hong-Wei Yang, Shuren Wang and Chen Cao

Received: 16 March 2023
Revised: 28 March 2023
Accepted: 28 March 2023
Published: 29 March 2023

1. Introduction

With the non-stop expansion of mining depth, flooring heave has emerged as one of the foremost traits and varieties of deformation and failure of surrounding rock in gentle rock. And it does great damage to the shape of the roadway. The discount of roadway sections precipitated utilizing ground heave poses a big danger to the security manufacturing of the mine [1–3]. The stress of the surrounding rock of the roadway can be significantly reduced by anchoring the occurrence position of floor heave by the direct bottom control method. Still, the rock mass of a hole wall is easy to collapse, which frequently leads to the accumulation of gravel sediment in the backside of the hole, which brings a huge problem for the installation of the anchor cable [4]. Eventually, this leads to the incidence of disasters.

At present, the most commonly used anchor cable installation method is manual installation, which can be manually adjusted to install the anchor cable to the bottom of the hole when encountering residue accumulated at the bottom of the hole. However, the environment is harsh when the anchor cable is installed, the work intensity of the workers is high and the efficiency is low [5,6]. The method of installing the drill bit in the front section of the anchor cable was proposed. It is of great significance to improve the drilling efficiency and structural optimization of anchor cables.

A number of studies have been conducted on drill bits. Cooley [7] analyzed the heat generation phenomenon in the process of using spiral bits and proposed that the drilling speed, length and diameter of the drill bit are the main factors affecting the drilling temperature. Saha [8] designed a new type of spiral bit, studied the influence of constant feed speed and thrust on the peak temperature of a spiral drill, and analyzed the impact of the spiral blade and tip angle of different types of bit on cutting.

Kim studied the influence of the characteristics of the drill bit and the change in drilling conditions on the drilling force and stress distribution of the drill bit, which furnished a theoretical groundwork for optimizing the geometry of the drill bit [9]. Zhang [10] designed a PRF drill bit. Compared with the traditional twist drill, it was found that the resistance of the improved PRF drill bit was reduced by 23.8% on average under the same cutting conditions. According to the characteristics of bit materials and rock materials, Šporin [11] reveals the wear mechanism of a bit under given rock materials and drilling conditions. Yakym [12] conducted a metallographic analysis of several steel materials commonly used in drill bit production and discussed the methods to prevent premature loss of drill bit workability. Šporin [13] used an optical microscope to analyze the drill bit material's chemical composition and the rock material's mechanical parameters. The research results laid a good foundation for developing new alloy drill bits. Moura [14] developed a new drilling performance prediction model and determined the linear relationship between the 'drillability constant' of the Maurer model and the bit weight on a bit.

However, the drilling bit research mainly focuses on the drilling of solids, and drilling research in granular particles are relatively few.

Scholars have also done a lot of research on the movement of particles. Due to the complexity and randomness of the movement of particulate matter, particulate matter presents some unique properties, different from solids, gases and liquids. Utter [15] conducted the shear test of dense granular materials on the two-dimensional Couette geometric model. It was found that when the thick, fine material is sheared, shear bands and anisotropic force chain networks will be formed. Antony [16] studied the collective behavior of three-dimensional granular media. He found that particles' filling rate and geometric stability are inversely proportional to the friction coefficient and elastic modulus between particles. Daniel Barreto [17] explored the effect of the friction coefficient between particles on the properties of granular materials by the discrete element method. It was found that an increase in friction coefficient can significantly enhance the internal stability of the particle force chain. Senetakis [18] conducted a micro-mechanical sliding test at the contact of broken limestone particles to capture the friction response during steady-state sliding. It was found that there was no significant difference in the friction response between the dry state and the oil-immersed state. Sandeep [19] studied particles' elastic properties and surface morphology's influence on the friction between particles through experiments. It was found that the friction coefficient between particles was negatively correlated with Young's modulus and surface roughness.

Multi-body dynamics (MBD) software has good kinematics analysis ability, but cannot complete the construction of a particle working environment. In 1971, Cundall [20,21] proposed an evaluation approach (DEM) for discrete granular substances, primarily based on molecular dynamics theory. Nowadays, the co-simulation method through DEM-MBD is more mature. Ren [22] used ADAMS-EDEM joint simulation to study the dynamic characteristics of the scraper conveyor under partial load and variable load conditions. The outcomes confirmed that the lateral vibration of the scraper chain used to be positively correlated with the quantity of coal transported, and the longitudinal vibration was once negatively correlated with the quantity of coal transported. Jiang [23] et al. used a DEM-MBD co-simulation to simulate and analyze the dynamic characteristics of the chain drive system under different impact loads and obtained the chainrings and the scraper's vibration under impact load. It provides a reference for the structural optimization and fault diagnosis of scraper conveyors. Shi [24] used DEM-MBD to study ballast damage during tamping. Nowadays, the joint simulation of DEM-MBD has been widely used in engineering machinery [25].

Therefore, combined with the above problems, and drawing on the research results of scholars, this paper proposes a drill anchor cable installation method, and uses DEM-MBD co-simulation and test methods to analyze the main factors affecting the drilling performance of the anchor cable: axial speed, feed rate, anchor cable pitch and working

aperture. The dynamic traits of the drill anchor cable setup approach at some points of drilling are studied.

2. Research Method

2.1. Contact Model

In discrete element modeling, the Hertz-Mindlin (no-slip) contact model is most frequently employed. Figure 1 depicts the model's schematic layout.

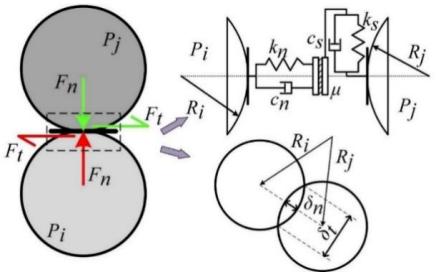

Figure 1. Hertz–Mindlin (no-slip) contact model.

The normal force in the model can be given by Equation (1):

$$F_n = \frac{4}{3} E^* \sqrt{R^*} \delta_n^{\frac{3}{2}} \tag{1}$$

where E^* is the equivalent of Young's modulus, R^* is the equivalent radius and δ_n is the standard overlap.

The identical Young's modulus E^* and equivalent radius R^* are given by Equations (2) and (3), respectively:

$$\frac{1}{E^*} = \frac{\left(1 - v_i^2\right)}{E_i} + \frac{\left(1 - v_j^2\right)}{E_j} \tag{2}$$

$$\frac{1}{R^*} = \frac{1}{R_i} + \frac{1}{R_j} \tag{3}$$

where E_i, v_i, and R_i, E_j, v_j and R_j are Young's modulus, and Poisson's ratio and radius of particles i and j are in contact with each other, respectively.

2.2. DEM Particle Parameters

In the DEM numerical simulation process, DEM particle parameters have an important influence on the motion state of particles, so it is necessary to calibrate the particle-related parameters before simulation. As shown in Figure 2, the relevant parameters of the particle were calibrated through cylinder pulling, slope, rolling and drop experiments. The average diameter of the gravel is 7.4 mm.

The cylinder pulling experiment was used to calibrate the angle of repose of the particle, the slope experiment was used to calibrate the static friction coefficient between gravel and the anchor cable, and the rolling experiment was used to calibrate the rolling friction coefficient between a rock and the anchor cable. The drop experiment was used to calibrate the restitution coefficient of the gravel particle. The DEM parameters after calibration are shown in Table 1. In this table, density, Poisson's ratio and shear modulus are P, σ and G, respectively. The coefficients of recovery, static friction and rolling friction are η, μS and μR, respectively.

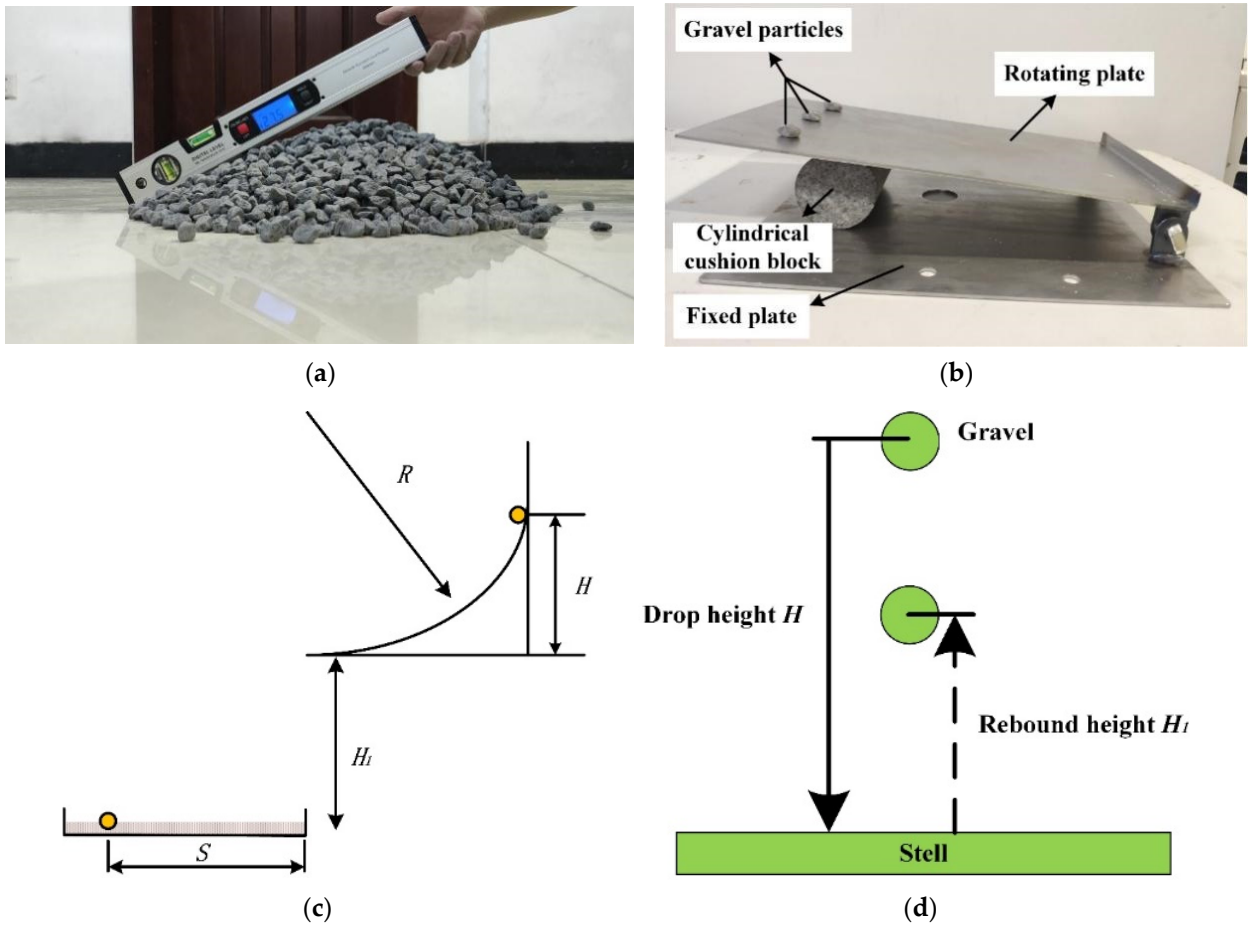

Figure 2. Calibration experiment of DEM particle parameters: (**a**) cylinder pulling experiment, (**b**) slope experiment, (**c**) rolling experiment, (**d**) drop experiment.

Table 1. The parameters of DEM.

	G (GPa)	P (kg/m^3)	σ		μR	η	μS
Gravel	11	2700	0.29	Gravel—Gravel	0.2	0.62	0.74
Anchor cable	8.02	7801	0.29	Gravel—Anchor cable	0.25	0.42	0.49

2.3. Construction Model

2.3.1. Build A Test-Bed

The drill bit anchor cable drilling test bench built in this article is shown in Figure 3.

In the experiment, the organizational activities of the mechanical module are regulated by the control module. In the automatic module, the screw motor provides the low feed speed of the anchor cable, and the rotating motor provides the axial velocity of the anchor cable. When the bit anchor cable is drilling, the drilling resistance and torque data are transmitted to the data analysis module through the data acquisition instrument to process and analyze the signal.

2.3.2. Simulation Model

The simulation model is shown in Figure 4. The bottom of the anchor cable in the figure is a conical drill structure. According to the shape and size of gravel sediment in a bottom hole, a suitable gravel particle model was constructed using DEM software. Then, through the DEM software, a cylindrical hole-like workspace was generated. Simulation requirements determined the aperture and height. The DEM generated gravel particles were placed for 5S until they reached a stable state. The particle depth is 0.52 m, the particle

diameter is 7.4 mm, and the working aperture is 160 mm. The Hertz–Mindlin (no-slip) contact modle is adopted between particles. The mannequin of the anchor cable is built in MBD software, and DEM-MBD is used for joint simulation.

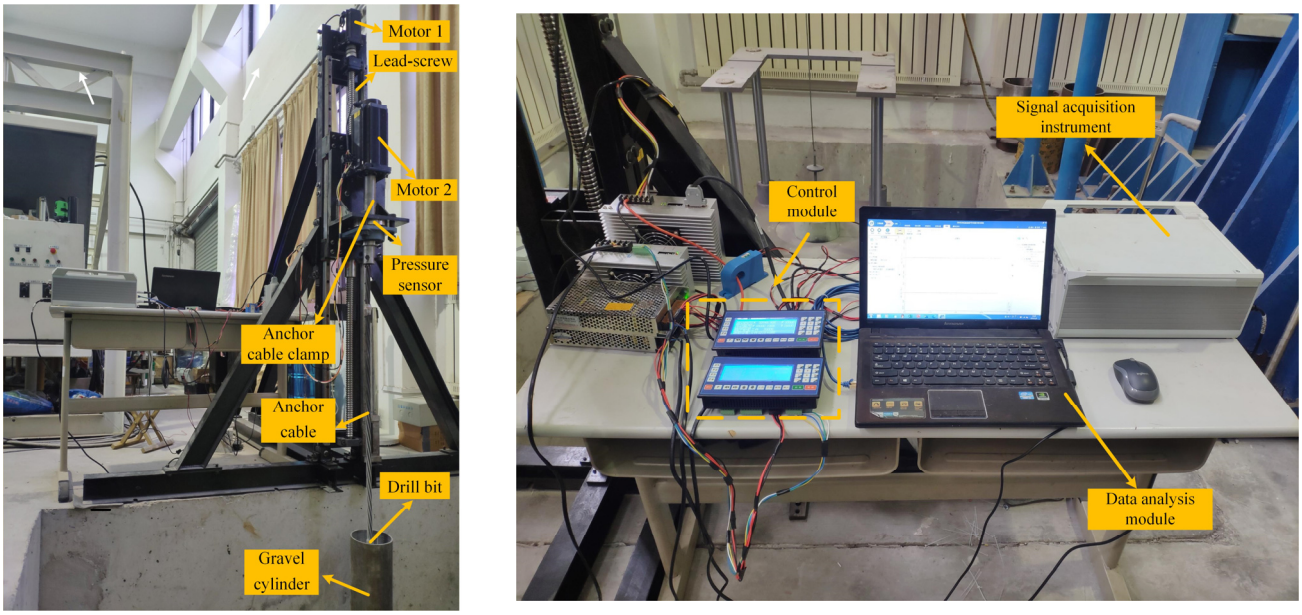

Figure 3. Test-bed structure diagram; (**a**) Mechanical module; (**b**) Control and data acquisition module.

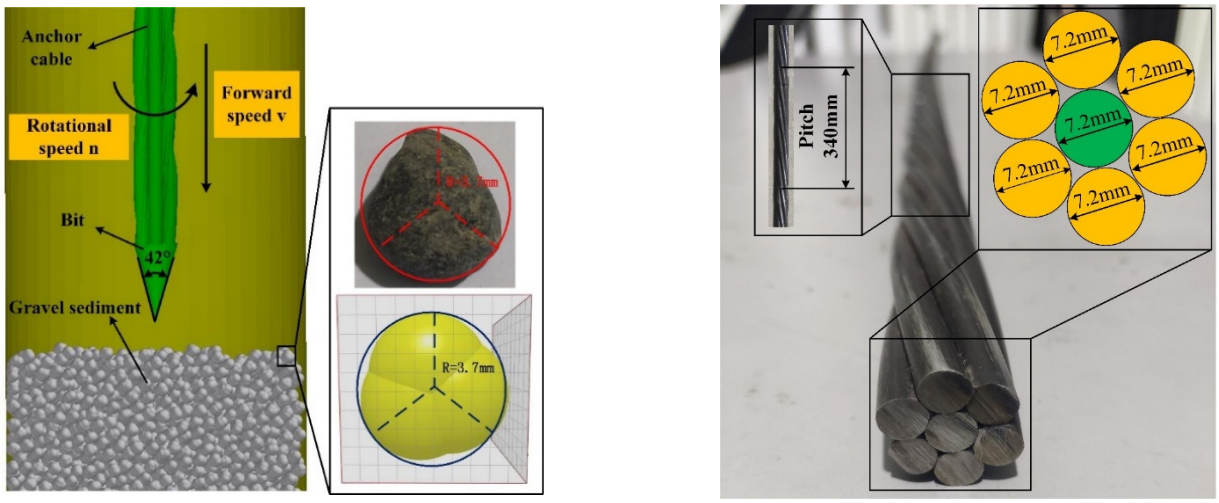

Figure 4. The bit anchor cable; (**a**) simulation model; (**b**) anchor cable.

2.4. Feasibility Analysis of Bit Anchor Cable Installation Method

In this paper, the feasibility of the proposed anchor cable installation method is verified by discrete element-multibody dynamics co-simulation. The conventional drill-less anchor cable and the drill bit anchor proposed in this paper are compared and analyzed, and the simulation result is shown in Figure 5. The control feed speed is 0.03 m/s and the axial speed is 0.60 rpm. In the process of signal acquisition, the pressure sensor in Figure 3a sensed the pressure signal, and then the signal acquisition instrument in Figure 3b inputted the collected pressure signal to the data analysis module.

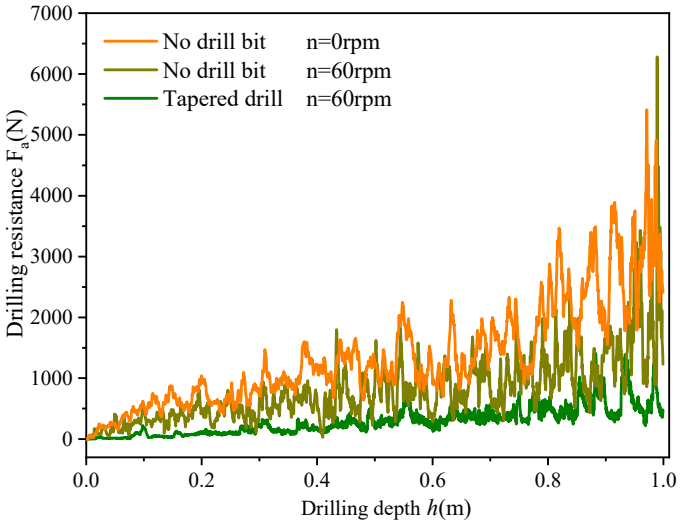

Figure 5. Comparison diagram of drilling resistance.

When the speed is 0 rpm, the drilling resistance is extremely high when drilling without a drill bit anchor cable, and the growth rate of drilling resistance is 2678; when the speed is 60 rpm, the drilling resistance growth rate of the drill-less anchor cable is reduced by 42%, but the drilling resistance of the anchor cable is still large.

When drilling with a drill bit anchor cable, the resistance of the anchor cable is significantly reduced. At 60 rpm, the resistance of the drill bit anchor cable increases by 61%, compared to the drill-less anchor cable during drilling. It can be seen that the drill bit anchor cable proposed in this paper can effectively reduce the drilling resistance during anchor cable installation, and then verify the feasibility of this method.

2.5. Research Program

To further explore the dynamic characteristics of the bit anchor cable under different working conditions, the main factors affecting the drilling performance of the drill anchor cable are analyzed and studied: axial speed, feed rate, anchor cable pitch and cylinder working space aperture. Experimental variables are shown in Table 2.

Table 2. Experimental scheme variable table.

Axial Speed/rpm	Feed Rate/(m/s)	Anchor Cable Pitch/mm	Working Aperture/mm
0, 120, 240, 360	0.03, 0.06, 0.09, 0.12	140, 240, 340, 440, 540	80, 120, 160, 200, 240

3. Results and Discussion

3.1. Axial Speed

The drill bit anchor cable drilling resistance curve is shown in Figure 6. It can be found that as the drilling depth of the drill bit anchor cable increases, the drilling resistance is an upward curve that first increases slowly and then increases rapidly. When the speed is n = 0 rpm, the drilling resistance of the drill bit anchor cable is significantly higher than that of n = 120, 240 and 360 rpm. It can be concluded that the rotational speed has a restraining effect on the resistance of the drill bit anchor cable during drilling. At the same time, it can be seen that the effect on the change of resistance after increasing the speed from 240 rpm to 360 rpm is much less than that of increasing the speed from 120 rpm to 240 rpm.

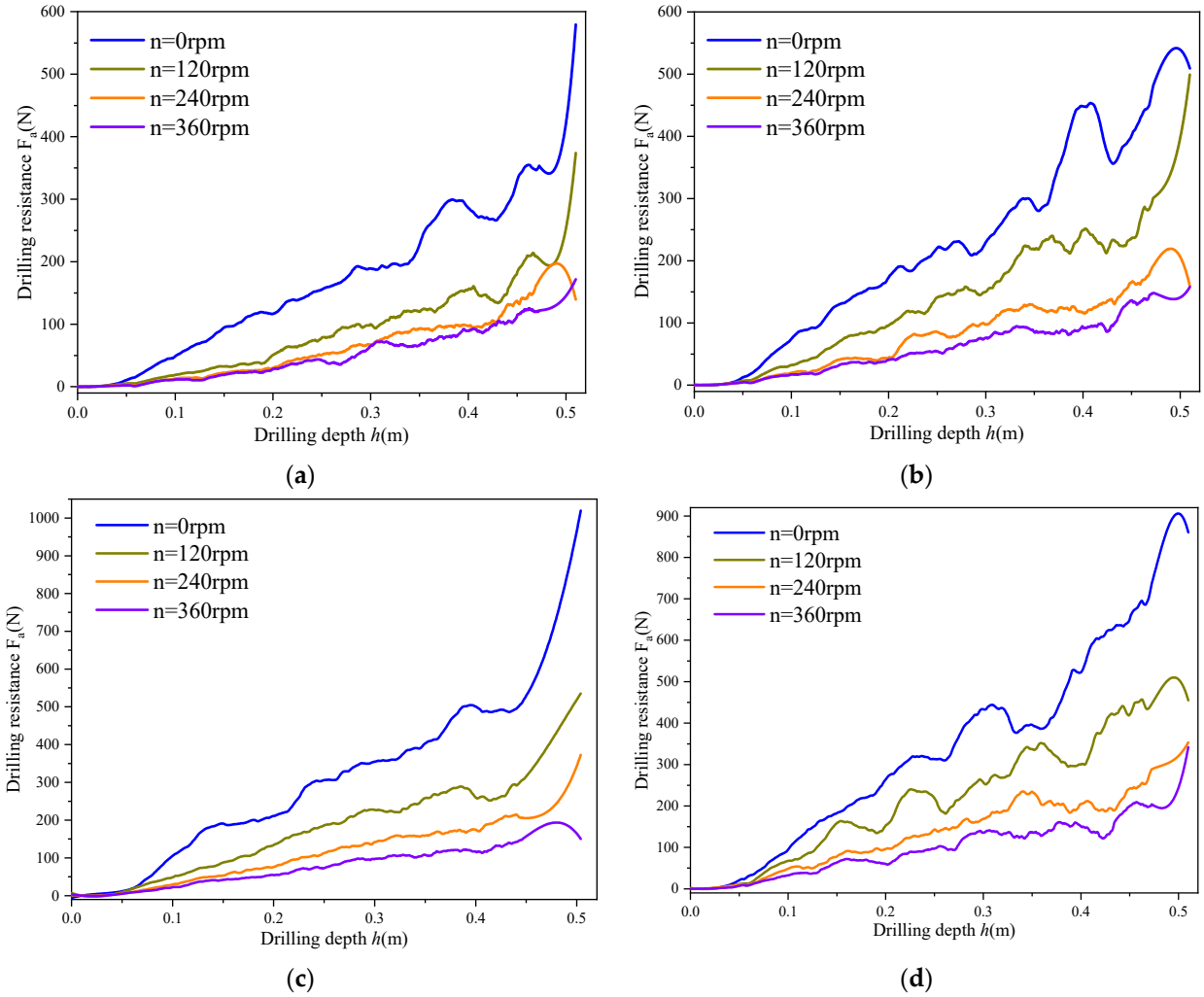

Figure 6. Drilling resistance curves of drill anchor cable under different axial speeds; (**a**) v = 0.03 m/s; (**b**) v = 0.06 m/s; (**c**) v = 0.09 m/s; (**d**) v = 0.12 m/s.

To further explore the reasons for the influence of speed on the dynamic characteristics of the drill bit anchor cable during the drilling process, the drill bit anchor cable feed speed was controlled to 0.03 m/s, and the velocity vector of the bottom hole gravel sediment particles under different axial speeds was analyzed. When the drill bit anchor cable is drilled to a depth of 0.4 m, the particle velocity vector plot is shown in Figure 7.

Affected by the screw structure, when the drill bit anchor cable is drilled, the structure of the bolt will constantly pull the surrounding gravel particles upward, so that the particles have an upward-moving trend. The upward movement of the particles will give the downward reaction force to the spiral structure of the drill anchor cable. It can be viewed from Figure 7 that, with the extent of the rotation pace of the drill anchor cable, the variety of upwardly shifting particles around the drill anchor cable and the speed of the particles progressively increase. Therefore, this will give the bit anchor cable a downward thrust. Finally, the drilling resistance of the drill anchor cable in Figure 6 regularly decreases with the amplification in rotation speed.

Figure 8 indicates the simulation and check curves when the feed fee is 0.03 m/s. It can be observed from the parent that, as the rotation pace increases, the drilling resistance of the drill anchor cable progressively decreases. Therefore, the correctness of the simulation is verified.

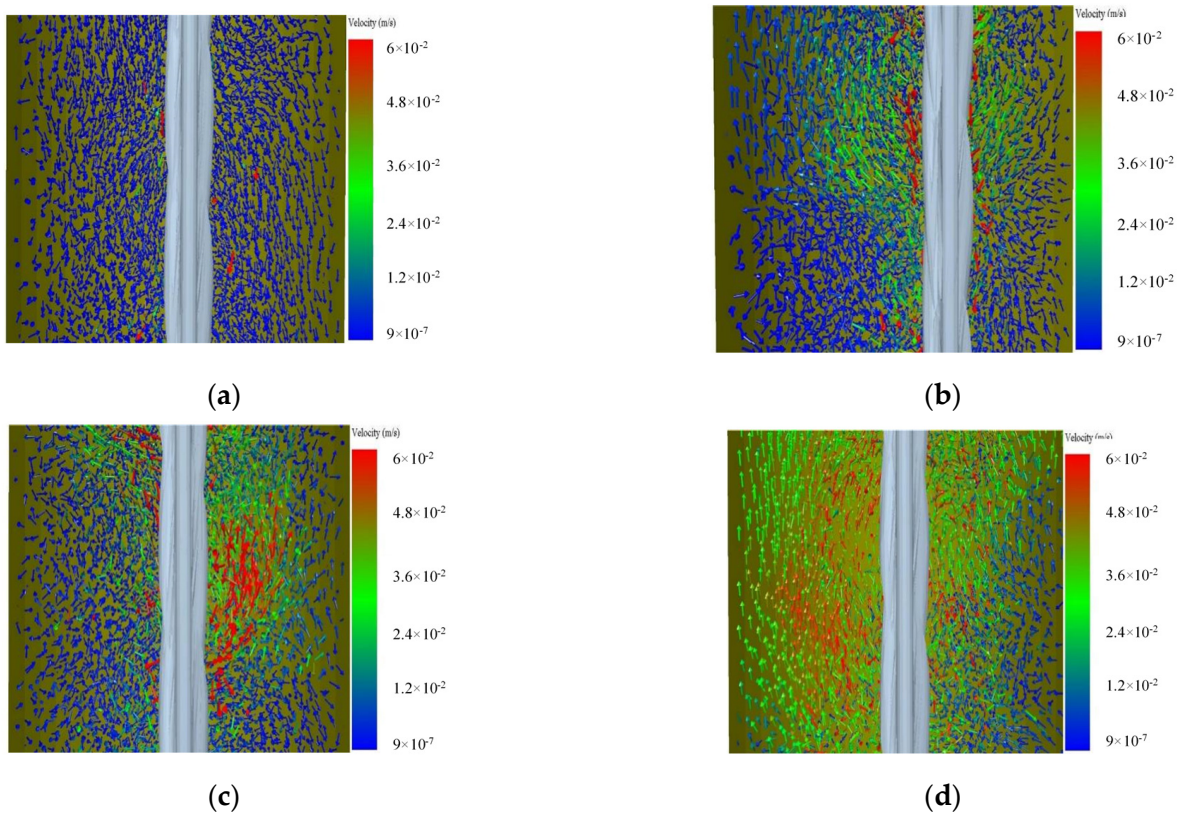

Figure 7. Vector diagram of particle motion around bit anchor cable at different rotation speeds; (**a**) n = 0 rpm; (**b**) n = 120 rpm; (**c**) n = 240 rpm; (**d**) n = 360 rpm.

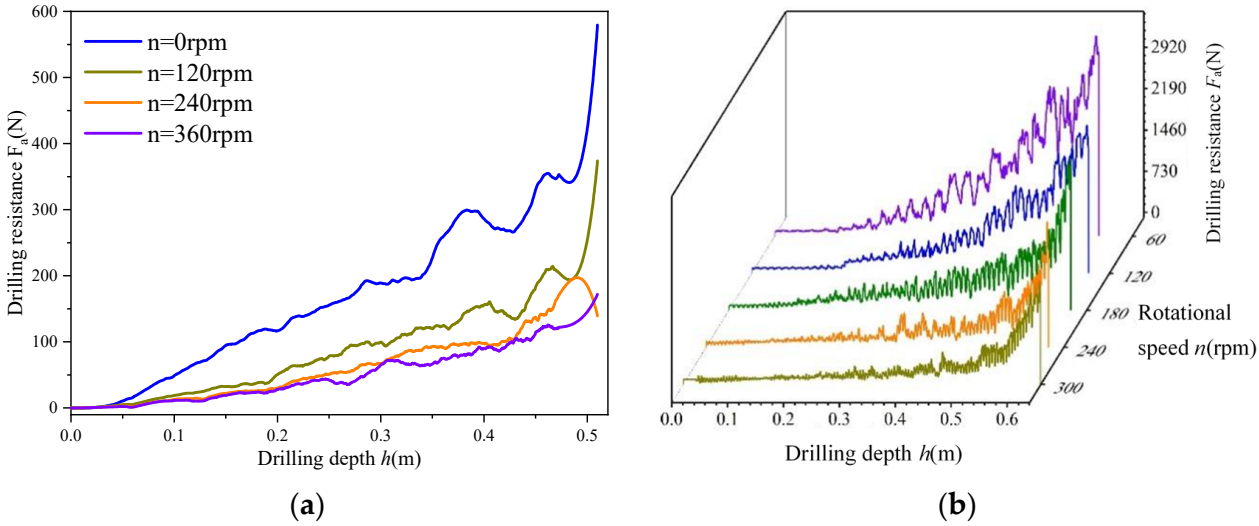

Figure 8. Verify the simulation model: (**a**) Simulation curve; (**b**) Test curve.

3.2. Feed Rate

To explore the influence of feed rate on drill bit anchor cable during drilling, the axial speed of the drill bit anchor cable is set to 0, 120, 240 and 360 rpm, respectively, and different feed speeds are controlled to simulate anchor line drilling. The drilling resistance change curve of the obtained drill bit anchor cable during operation is shown in Figure 9.

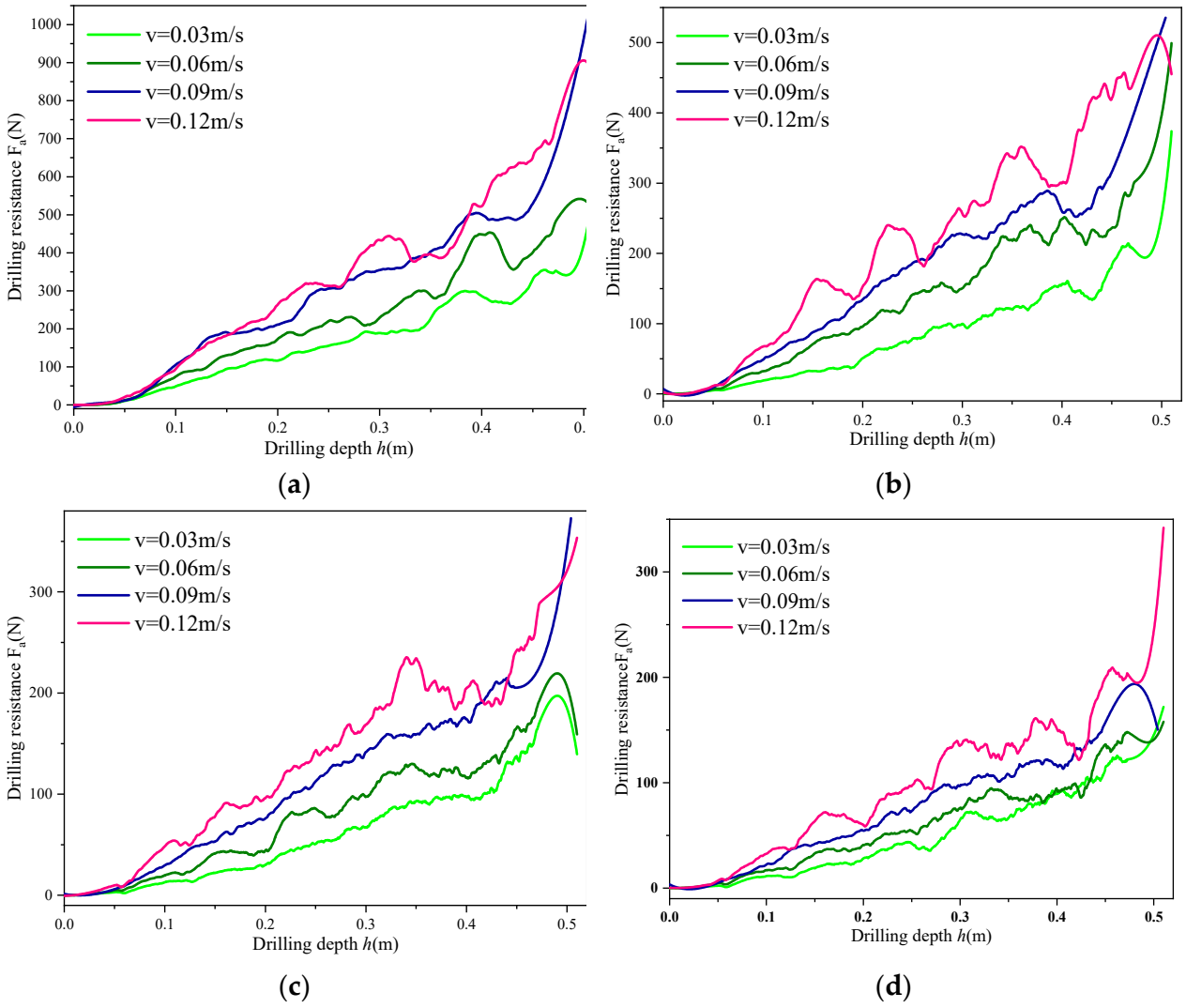

Figure 9. Resistance curve of bit anchor cable drilling below exclusive feeding rates: (**a**) n = 0 rpm; (**b**) n = 120 rpm; (**c**) n = 240 rpm; (**d**) n = 360 rpm.

It can be seen from Figure 9 that, under the same axial speed, with the increase of feed speed, the resistance of the drill bit anchor cable during operation gradually increases. To reflect the influence of feed rate on drilling resistance more obviously, the curve of Figure 9 is fitted, the fitted line is y = a + bx, and the fitted R^2 is greater than 0.95. The slope is counted, as shown in Table 3, and the data in the Table is plotted as a curve, as shown in Figure 10. It can be considered from the discern that, at the identical speed, the slope of the geared-up straight line of the drilling resistance of the bit anchor cable is positively correlated with the feed charge of the bit anchor cable. The smaller the rotation speed of the drill anchor cable, the stronger the positive correlation between the slope of the fitting line and the feed rate of the bit anchor cable. When the feed charge of the bit anchor cable is 0.12 m/s and the rotation velocity is zero rpm, the slope of the becoming line of the drilling resistance of the bit anchor cable is 715 greater than that at the identical rotation velocity when the feed fee is 0.03 m/s. When the feed charge of the bit anchor cable is 0.12 m/s and the rotation velocity is 360 rpm, the slope of the becoming line of the drilling resistance of the bit anchor cable is solely 183 greater than that at the identical rotation pace when the feed charge is 0.03 m/s.

Table 3. Fitting straight line slope table of drilling resistance.

Rotating Speed (rpm)	Feeding Rate (m/s)	Fitting Straight Line Slope	Rotating Speed (rpm)	Feeding Rate (m/s)	Fitting Straight Line Slope
0	0.03	698	240	0.03	272
0	0.06	933	240	0.06	381
0	0.09	1153	240	0.09	475
0	0.12	1413	240	0.12	555
120	0.03	374	360	0.03	222
120	0.06	595	360	0.06	254
120	0.09	747	360	0.09	328
120	0.12	908	360	0.12	405

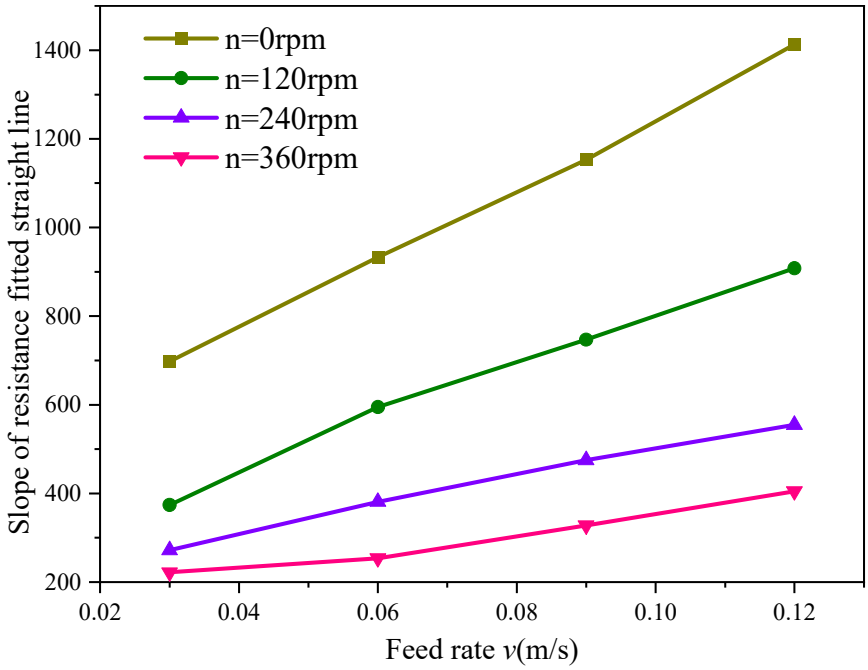

Figure 10. Comparison diagram of fitting straight line slope of bit anchor cable drilling resistance under different feeding rates.

To further explore the influence of feed rate on drill bit anchor cable during drilling, the DEM software program used to be used to export the speed vector layout of particles in the gap when the bit anchor cable used to be simply drilled to the backside of the gap at 360 rpm and with one-of-a-kind feed rates, as proven in Figure 11. When the feed rate is 0.03 m/s, the quicker particles in the gap are spirally disbursed round the drill anchor cable. With the feed price increase, the quicker particles' spiral distribution phenomenon gradually weakens and progressively turns into a vertical motion downwards, alongside the bit anchor cable. The stirring effect of the drill bit anchor cable on the particles in the hole is negatively correlated with the feed rate.

3.3. Anchor Cable Pitch

The stirring effect of the drill bit anchor cable on the particles in the hole is negatively correlated with the feed rate. In addition, the structure also has an unavoidable influence on the resistance of the drill bit anchor cable during drilling, and it is necessary to study the dynamic characteristics at different pitches.

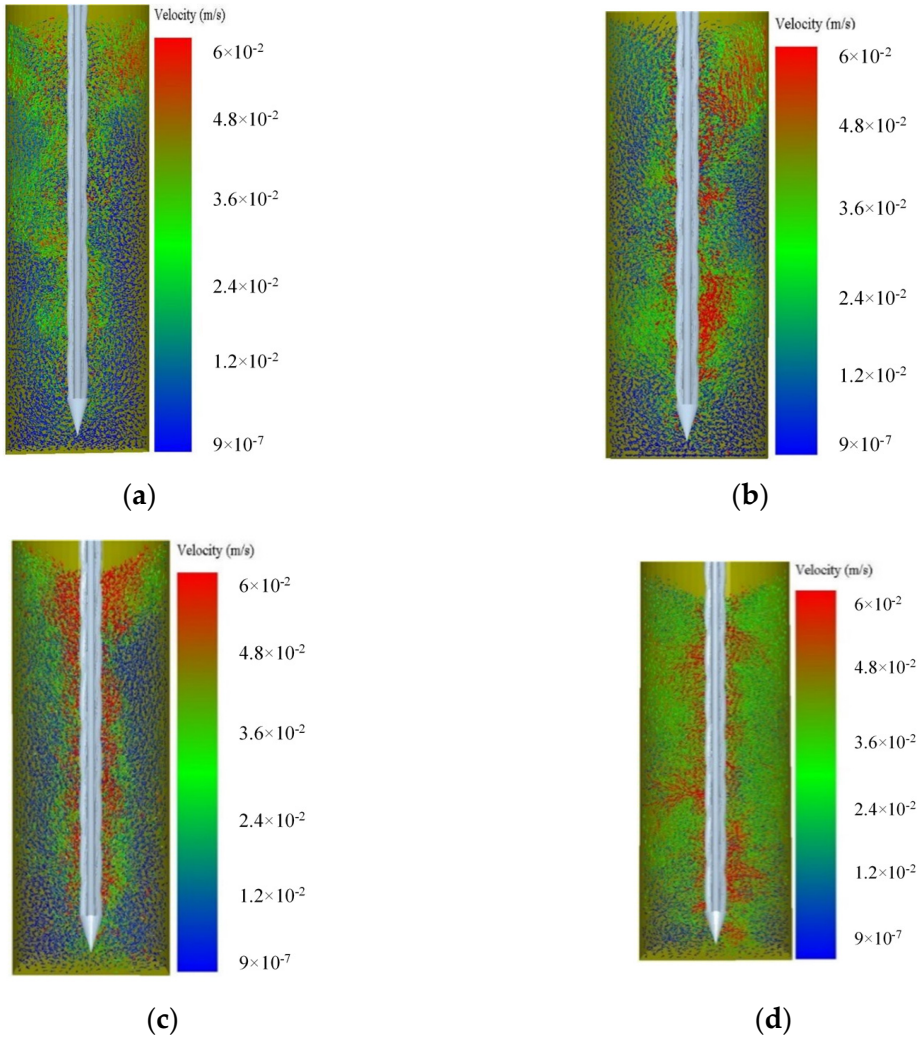

Figure 11. Vector diagram of particle motion state in the hole at different feeding rates: (**a**) v = 0.03 m/s; (**b**) v = 0.06 m/s; (**c**) v = 0.09 m/s; (**d**) v = 0.12 m/s.

As shown in Figure 12, five kinds of anchor cables with different pitch were designed, and drilling experiments were conducted on these five kinds of anchor cables, respectively. Then, the drilling simulation was carried out underneath special action parameters. The 340 mm pitch is the common pitch of the anchor cable.

In this paper, the resistance of the drill bit anchor cable under different pitches is linearly fitted during the drilling process, and the fitted R^2 is greater than 0.95. Figure 13 is the slope diagram of the provided straight line of the drilling resistance of the bit anchor cable at the feed rate of 0.06 m/s, and the feed rate of 0.12 m/s under different pitches.

It can be seen from Figure 13 that, when the pitch of the drill bit anchor cable is less than 440 mm, the growth rate of resistance experienced by the drill bit anchor cable during drilling is proportional to the pitch. When the pitch is greater than 440 mm and less than 540 mm, the growth rate of drilling resistance is inversely proportional to the pitch, and when the pitch reaches 440 mm, the growth rate of drilling resistance is the fastest.

Therefore, when the pitch is lower than 450 mm, the resistance value during drilling can be reduced by reducing the screw pitch of the drill bit anchor cable, which is consistent with the research conclusions of the literature [8], which shows that different sizes of the pitch have an important impact on the dynamic characteristics during drilling.

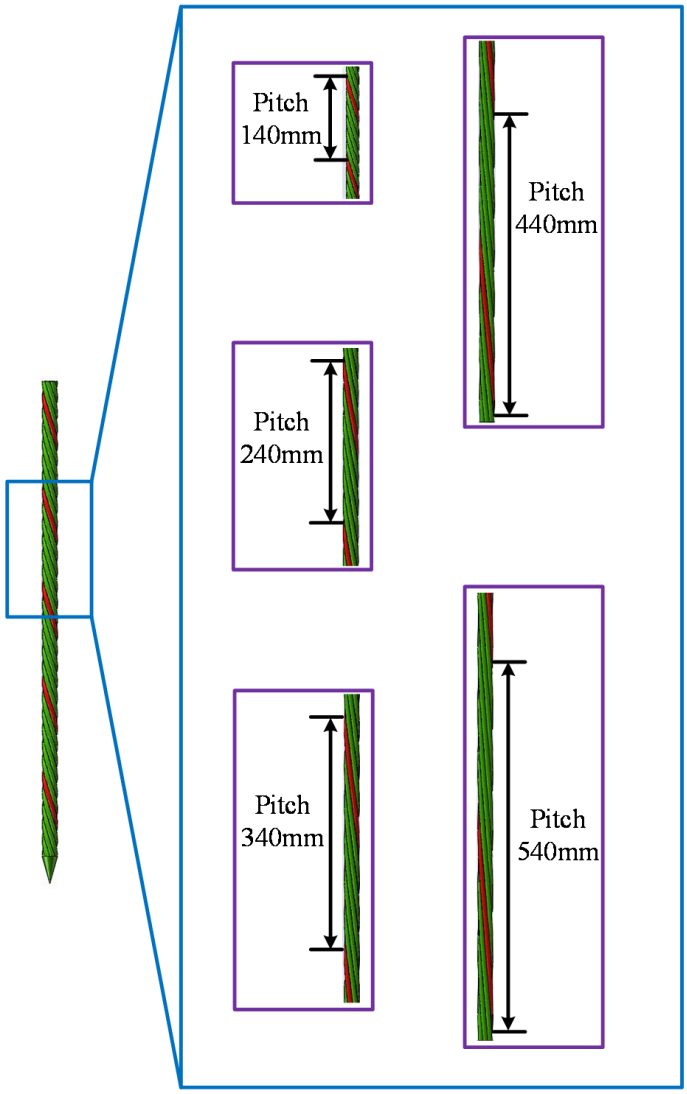

Figure 12. Structural design drawing of bit anchor cable pitch.

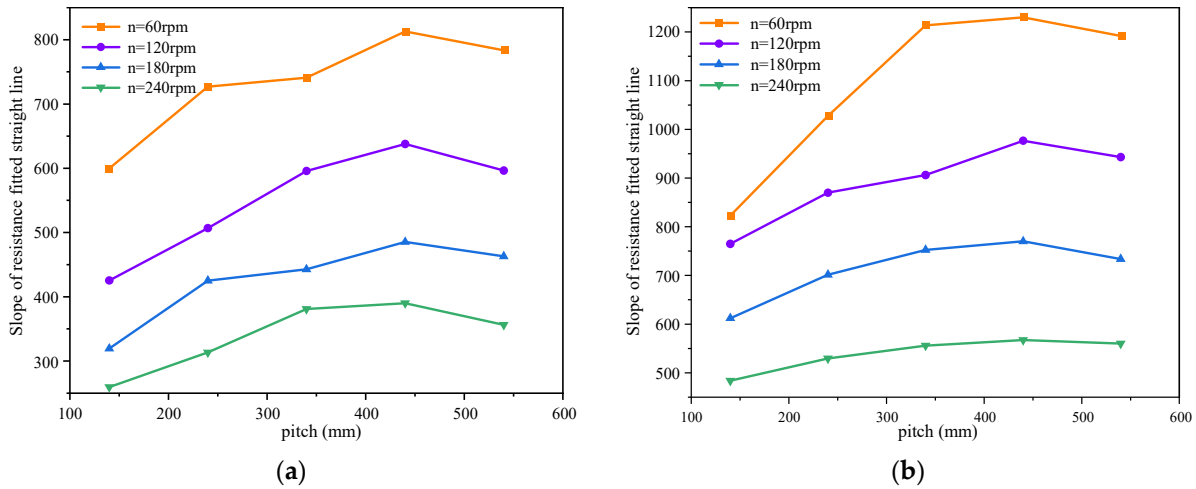

Figure 13. Fitting straight line slope diagram of drilling resistance of bit anchor cable under different pitches: (**a**) v = 0.06 m/s; (**b**) v = 0.12 m/s.

3.4. Working Aperture

Due to the influence of geological conditions and roadway deformation in different roadways, the aperture required for the installation of bit anchor cables will also be quite different. This section uses an experimental approach to investigate the effect of pore size on anchor cable drilling. The gravel container of the test bench is shown in Figure 14. There are five gravel containers with apertures of 80 mm, 120 mm, 160 mm, 200 mm and 240 mm, respectively. The relevant experimental variables are shown in Table 4. The particle depth in the cylindrical working hole is 800 mm. As shown in Figure 15, the drilling resistance and hindrance torque curves of the anchor cable under this operating condition are shown. At a drilling depth of around 0.5 m, the average of the drilling resistance and hindering torque during drilling is shown in Figure 16.

It can be seen from Figures 15 and 16 that, with the increase in the hole diameter, the drilling resistance and hindrance torque of the anchor cable during the drilling process gradually decrease. When the hole size varies between 80–120 mm and 160–240 mm, the reduction in drilling resistance and hindering torque is relatively small; when the bore size is changed from 120 mm to 160 mm, the drilling resistance and obstacle torque are significantly reduced.

The length of the anchor cable in this experiment is 1.5 m. The stiffness of the anchor cable has a certain relationship with the depth of the anchor cable into the gravel, which will be studied later.

As the drilling depth increases, the tightness between particles gradually increases, which is one reason for the increase in drilling resistance and hindering torque of the bit anchor cable. However, this reason will not lead to a rapid increase in drilling resistance. The reason for the rapid increase in drilling resistance is due to the inability of particles to move longitudinally.

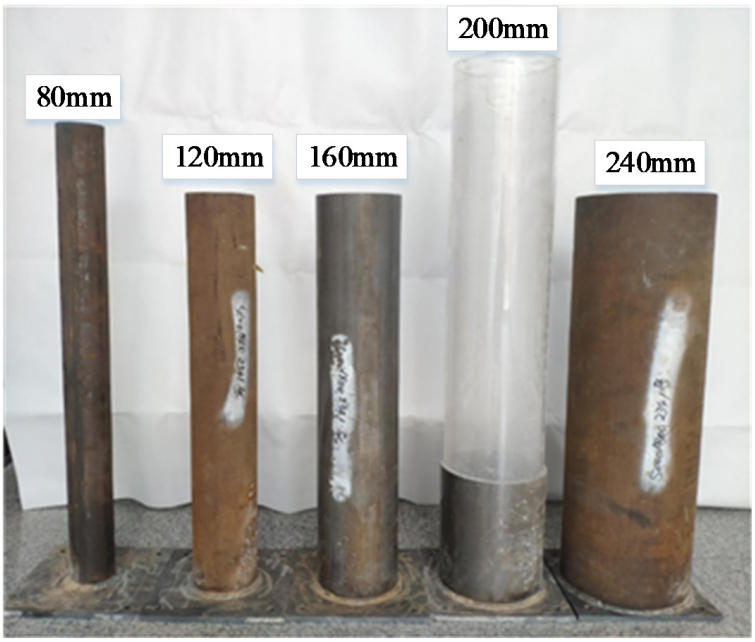

Figure 14. Gravel containers with different working apertures.

Table 4. Aperture simulation variable table.

Feeding Rates (m/s)	Axial Speed (rpm)	Aperture (mm)	Particle Depth in the Hole (mm)
0.01	240, 300	80, 120, 160, 200, 240	800

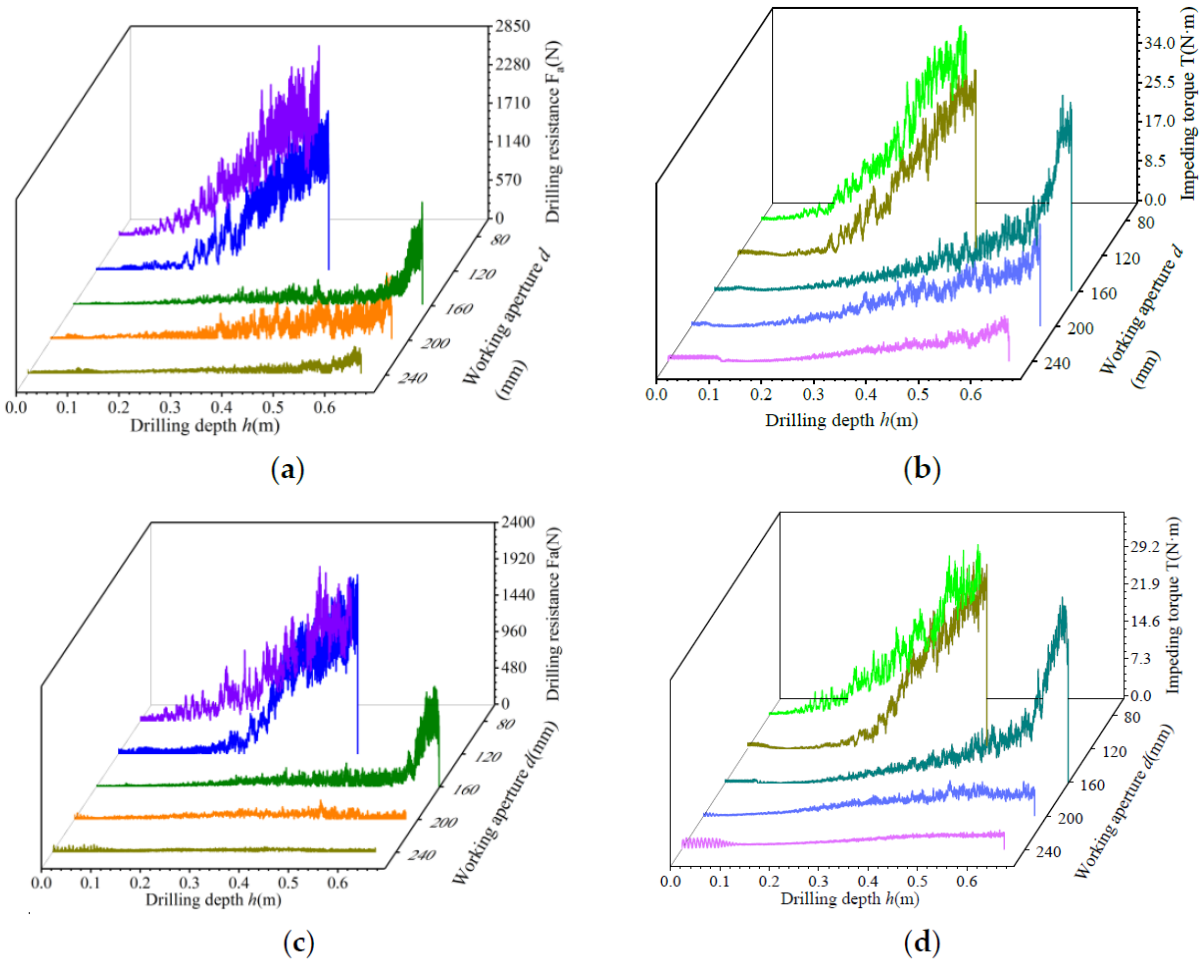

Figure 15. Dynamic features curve of bit anchor cable below amazing apertures: (**a**) n = 240 rpm Drilling resistance; (**b**) n = 240 rpm Hinder torque; (**c**) n = 300 rpm Drilling resistance; (**d**) n = 300 rpm Hinder torque.

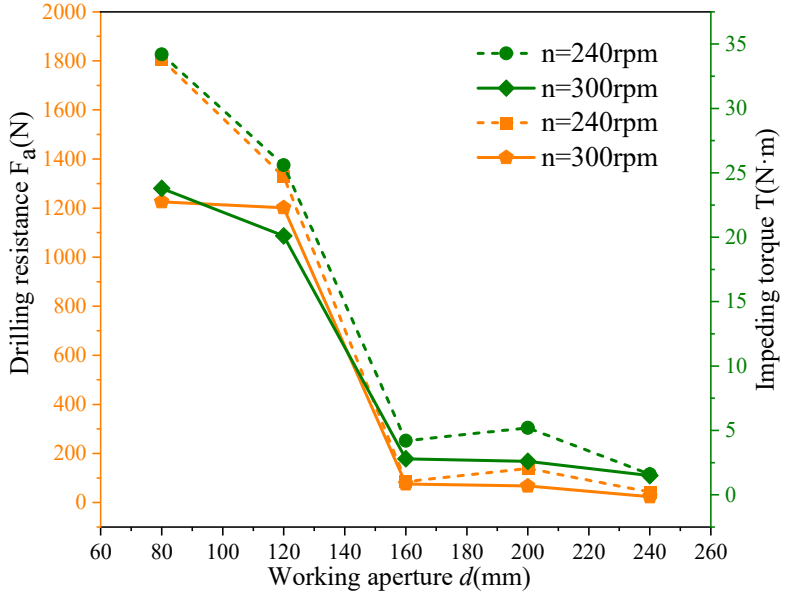

Figure 16. The average value of particle obstruction at different apertures and drilling depths of 0.5–0.55 m.

When the bit anchor cable is drilling, the particles under the bit mainly move in two directions, namely lateral movement and longitudinal movement. However, the space between the bit and the bottom of the hole is limited and, when the bit is near the bottom of the hole, it is difficult for the particles below the bit to move down. The bit anchor cable directly presses against the particles, resulting in a sharp increase in drilling resistance. Figure 17 provides a good illustration of this phenomenon.

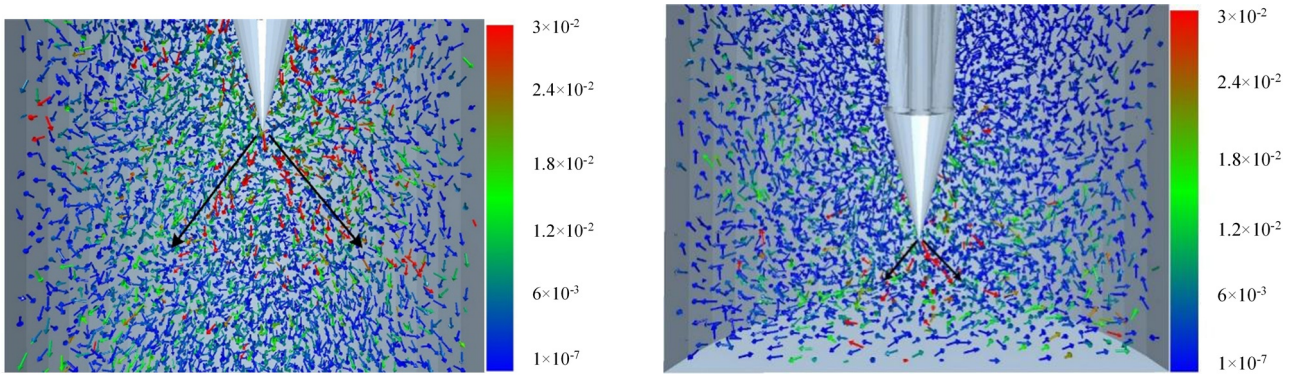

(**a**) (**b**)

Figure 17. Velocity vector diagram of particles at the lower end of the bit: (**a**) Particle velocity vector diagram when the bit is 0.2 m from the bottom of the hole; (**b**) Particle velocity vector diagram when the bit is 0.05 m from the bottom of the hole.

Figure 17 shows the velocity vector diagram of the particles at the lower end of the drill bit when the drill bit is drilled at different depths. It can be seen from this diagram that, when the drill bit is 0.2 m from the bottom of the hole, the velocity vector of the particles at the lower end of the drill bit show an apparent conical distribution. Under the extrusion of the drill bit, the particles below the drill bit will diffuse horizontally. At this time, the wide variety of particles that diffuse horizontally is large, and the increased fee of the drilling resistance of the drill bit anchor cable is extraordinarily slow. When the bit is 0.05 m away from the backside of the hole, the quantity of particles that endure lateral diffusion decreases sharply, and the drilling stress of the bit anchor cable directly acts on the backside of the gap via the particles, thereby inflicting the drilling resistance of the bit anchor line to push upward sharply.

4. Conclusions

In this paper, a new anchor cable installation method is proposed, and the feasibility of this method is verified. From the perspective of particle motion and anchor cable dynamics, the dynamic characteristics of bit anchor cable was studied. The following conclusions are drawn:

(1) Affected by using the spiral shape of the drill anchor rod, the axial velocity is negatively correlated with the drilling resistance of the bit anchor cable, and the effects are compared to confirm the correctness of the simulation. The pitch of the bit anchor thread has a hump-shaped relationship with drilling resistance. When the slope is much less than 450 mm, the drilling resistance can be decreased with the aid of appropriately lowering the pitch of the bit anchor cable;

(2) The feed speed is positively correlated with the resistance encountered during drilling; the degree of influence of the anchor cable on the particles in the hole is inversely correlated with the feed rate during drilling. The slope of the drilling resistance fitting line is positively correlated with the feed velocity, and the smaller the axial speed, the stronger the positive correlation between the slope and the feed speed;

(3) As the aperture increases, the drilling resistance and the hindering torque of the drill anchor cable gradually decrease. When the bit is 0.2 m away from the bottom of the

hole, the particle velocity vector at the lower end of the bit shows an evident conical distribution, and the particles diffuse horizontally. When the bit is 0.05 m from the bottom of the hole, the number of particles that diffuse laterally decreases sharply.

This paper is of great significance to the efficient installation of anchor cables and the protection against disasters. However, in practice, the anchor cable will have a certain degree of radial bending under the action of drilling resistance. The next step will be to use the finite element method to make the bolt model closer to the actual situation. Since the bit anchor cable needs to drill through gravel, it has certain requirements on the compressive strength of the gravel, which should be less than 30 Mpa.

Author Contributions: Formal analysis, K.G.; funding acquisition, K.G.; methodology, S.H., and X.L.; supervision, H.C., and J.L.; writing—original draft, H.C. and S.H.; writing—review and editing, H.C. and S.H. All authors have read and agreed to the published version of the manuscript.

Funding: This work was supported by the National Natural Science Foundation of China, grant number 52174146; the Project of Shandong Province Higher Educational Young Innovative Talent Introduction and Cultivation Team (Performance enhancement of deep coal mining equipment).

Institutional Review Board Statement: Not applicable.

Informed Consent Statement: Not applicable.

Data Availability Statement: Data were curated by the authors and are available upon request.

Conflicts of Interest: The authors declare no conflict of interest.

References

1. Hao, W.D.; Tao, D. Research on Deformation Control Technology of Broken Soft Rock Pre-mining Roadway. *IOP Conf. Ser. Earth Environ. Sci.* **2019**, *358*, 042047. [CrossRef]
2. Gao, Y.; Wang, C.; Liu, Y.; Wang, Y.; Han, L. Deformation mechanism and surrounding rock control in high-stress soft rock roadway: A case study. *Adv. Civ. Eng.* **2021**, *2021*, 9950391. [CrossRef]
3. Sun, Y.; Li, G.; Zhang, J.; Xu, J. Failure mechanisms of rheological coal roadway. *Sustainability* **2020**, *12*, 1885. [CrossRef]
4. Xu, Y.; Pan, K.; Zhang, H. Investigation of critical techniques on floor roadway support under the impacts of superimposed mining: Theoretical analysis and field study. *Environ. Earth Sci.* **2019**, *78*, 436. [CrossRef]
5. Shi, K.; Wu, X.; Tian, Y.; Xie, X. Analysis of re-tensioning time of anchor cable based on new prestress loss model. *Mathematics* **2021**, *9*, 1094. [CrossRef]
6. Yang, Z.P.; Li, S.Q.; Yu, Y.; Liu, X.; Hu, Y. Study on the variation characteristics of the anchor cable prestress based on field monitoring in a foundation pit. *Arab. J. Geosci.* **2020**, *13*, 1269. [CrossRef]
7. Cooley, R.L.; Barkmeier, W.W. Temperature rise in the pulp chamber caused by twist drills. *J. Prosthet. Dent.* **1980**, *44*, 426–429. [CrossRef]
8. Saha, S.; Pal, S.; Albright, J.A. Surgical drilling: Design and performance of an improved drill. *J. Biomech. Eng. Trans. Asme* **1982**, *104*, 245–252. [CrossRef]
9. Kim, K.W.; Ahn, T.K. Force Prediction and Stress Analysis of a Twist Drill from Tool Geometry and Cutting Conditions. *Int. J. Precis. Eng. Manuf.* **2005**, *6*, 65–72.
10. Zhang, Q.; Wang, J. Geometry, specification, and drilling performance of a plane rake-faced drill point design. *Proc. Inst. Mech. Eng. Part C J. Mech. Eng. Sci.* **2010**, *224*, 369–378. [CrossRef]
11. Šporin, J.; Mrvar, P.; Petrič, M.; Vižintin, G.; Vukelić, Z. The characterization of wear in roller cone drill bit by rock material—Sandstone. *J. Pet. Sci. Eng.* **2018**, *173*, 1355–1367. [CrossRef]
12. Yakym, R.S.; Petryna, D.Y. Analysis of Causes and Preventing Ways of Early Workability Loss of Three-Cone Rock Bit Cutters. *Met. Adv. Technol.* **2020**, *42*, 731–751. [CrossRef]
13. Porin, J.; Balako, T.; Mrvar, P.; Janc, B.; Vukeli, E. Change of the Properties of Steel Material of the Roller Cone Bit Due to the Influence of the Drilling Operational Parameters and Rock Properties. *Energies* **2020**, *13*, 5949.
14. Moura, J.D.; Xiao, Y.; Yang, J.; Butt, S.D. An empirical model for the drilling performance prediction for roller-cone drill bits. *J. Pet. Sci. Eng.* **2021**, *10*, 3287. [CrossRef]
15. Utter, B.; Behringer, R.P. Transients in sheared granular matter. *Eur. Phys. J.* **2004**, *14*, 373–380. [CrossRef]
16. Antony, S.J.; Kruyt, N.P. Role of interparticle friction and particle-scale elasticity in the shear-strength mechanism of three-dimensional granular media. *Phys. Rev. E* **2009**, *79*, 031308. [CrossRef]
17. Barreto, D.; O'Sullivan, C. The influence of inter-particle friction and the intermediate stress ratio on soil response under generalized stress conditions. *Granul. Matter* **2012**, *14*, 505–521. [CrossRef]

18. Senetakis, K.; Sandeep, C.S.; Todisco, M.C. Dynamic inter-particle friction of crushed limestone surfaces. *Tribol. Int.* **2017**, *111*, 1–8. [CrossRef]
19. Sandeep, C.S.; Senetakis, K. Effect of Young's Modulus and Surface Roughness on the Inter-Particle Friction of Granular Materials. *Materials* **2018**, *11*, 217. [CrossRef]
20. Cundall, P.A.; Strack, O.D.L. A discrete numerical model for granular assemblies. *Geotechnique* **2008**, *30*, 331–336. [CrossRef]
21. Cundall, P.A. The measurement and Analysis of accelerations in rock slopes. Ph.D. Thesis, University of London: Imperial College of Science and Technology, London, UK, 1971.
22. Ren, W.J.; Wang, L.; Mao, Q.H.; Jiang, S.B.; Huang, S. Coupling Properties of Chain Drive System under Various and Eccentric Loads. *Int. J. Simul. Model.* **2020**, *19*, 643–654. [CrossRef]
23. Jiang, S.B.; Huang, S.; Zeng, Q.L. Dynamic properties of chain drive system considering multiple impact factors. *Int. J. Simul. Model* **2022**, *21*, 284–295. [CrossRef]
24. Shi, S.; Gao, L.; Xiao, H.; Xu, Y.; Yin, H. Research on ballast breakage under tamping operation based on DEM–MBD coupling approach. *Constr. Build. Mater.* **2021**, *272*, 121810. [CrossRef]
25. Chen, Z.; Xue, D.; Wang, G.; Cui, D.; Fang, Y.; Wang, S. Simulation and optimization of the tracked chassis performance of electric shovel based on DEM-MBD. *Powder Technol.* **2021**, *390*, 428–441. [CrossRef]